Proceedings of the 2000 IEEE
International Conference on Robotics & Automation
San Francisco, CA • April 2000

# Kinematic design of a humanoid robotic shoulder complex

Jadran Lenarčič*, Michael M. Stanišić**, and Vincenzo Parenti-Castelli***

*Department of Automatics, Biocybernetics and Robotics
The "Jozef Stefan" Institute, Ljubljana, Slovenia

**Department of Aerospace and Mechanical Engineering
University of Notre Dame, Notre Dame, Indiana, USA

***DIEM – Faculty of Engineering
University of Bologna, Bologna, Italy

## Abstract

*In this paper, we present a mechanical design for a humanoid robotic shoulder complex. The aim of the mechanism is to support the load of the arm and to copy four principal motions of the human shoulder in order to furnish the desired arm mobility and reachability. We utilize a fully parallel mechanism with four driven legs that provide to the movable platform (on which the arm is to be attached) three rotations and one translation. These three rotations represent the shoulder's flexion-extension (about the vertical axis), the shoulder's abduction-adduction (about the anterior-posterior axis), and the shoulder's rotation (about the medial-lateral axis). The fourth degree of freedom is controlled depending on the angles of the first two rotations and represents the shoulder contraction and enlargement along the medial-lateral axis.*

## 1 Introduction

Today's robotic shoulders incorporate different types of spherical or universal joints representing the function of glenohumeral articulation [1,2]. In humans, however, the shoulder complex is an assemblage of three articulations, which are the sternoclavicular joint, the scapulothoracic joint, and the glenohumeral joint. The first two articulations connect the shoulder to the body, while the third one connects the upper arm to the shoulder. They are driven by a number of coupled actuators. Even though the first two joints possess relatively small ranges of motion if compared to the glenohumeral joint and other joints of the arm, their contribution to the arm performances is extremely important. The shoulder complex radically increases the arm's mobility and reachability by the use of the sternoclavicular and scapulothoracic degrees of freedom. This role of the sternoclavicular and the scapulothoracic joint in the human arm movement has been demonstrated in our previous works [3,4]. Recent investigations showed that they also enlarge the self-motion ability and the amount of positioning redundancy of the arm [5]. We can speculate that they additionally contribute to the arm's adaptability to adjust the manipulability, isotropy, compliance and other performance indices respecting the task requirements.

The objective of this article is to describe a design of a humanoid robotic shoulder mechanism simulating the function of the sternoclavicular and the scapulothoracic joint. In this work, we first mathematically formulate the kinematical properties of the human shoulder when modeled as a serial mechanism. In our design, however, we utilize a fully parallel mechanism with four driven extendable legs connecting a fixed base and a movable platform. It is understood that the base is attached to the body, while the upper arm is connected to the movable platform by a glenohumeral joint. The platform has four degrees of freedom; three are rotational and represent the shoulder's flexion-extension, the shoulder's abduction-adduction, and the shoulder's rotation. The fourth is a translation that can be associated with the shoulder's contraction along the clavicular axis that occurs during the arm elevation.

0-7803-5886-4/00/$10.00© 2000 IEEE


Authorized licensed use limited to: Universita degli Studi di Genova. Downloaded on April 29,2023 at 14:43:20 UTC from IEEE Xplore. Restrictions apply.

## 2 Principal kinematic aspects of the human shoulder complex

The human shoulder complex is made of a clavicle and scapula [1]. The clavicle is on one side attached to the sterna (anterior part of the body) by a spherical-type sternoclavicular joint, and on the other side to the scapula. The planar-type scapulothoracic joint enables the motion of scapula. The upper arm (humerus) is attached at the lateral end of the scapula by the spherical-type glenohumeral joint. In a first approximation [3], we can represent the shoulder complex as shown in Fig. 1. In this approximation, the inner articulation is concentrated in point S and simulates the sternoclavicular joint, the outer articulation is concentrated in point G and associated with the glenohumeral joint. The translation along the shoulder link represents the shoulder's enlargement. This is dependent on the inclination in the articulation about point S. The shoulder link between points S and G simulates the clavicle. The upper arm link is between points G and the elbow center E.

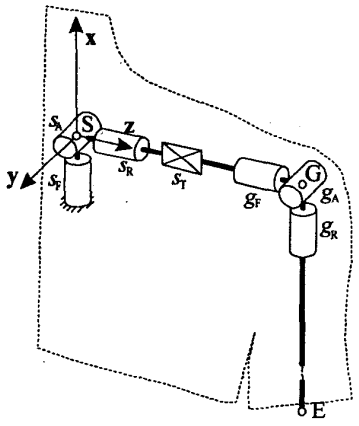


**Fig. 1**: *A serial model of the human shoulder complex*

In Fig 1, angles $s_F, s_A, s_R$ represent the shoulder flexion-extension, the shoulder abduction-adduction, and the shoulder rotation, while angles $g_F, g_A, g_R$ are the upper arm flexion-extension, the upper arm abduction-adduction, and the upper arm rotation, respectively. Linear coordinate $s_T$ is the shoulder translation. We assume that all coordinates are zero, if the mechanism's position is given as that in Fig. 1. Note that the listed joint coordinates and their upper and lower limits are coupled. Their interdependency is very complex and it is difficult to formulate it with precise mathematical functions. Some attempts, however, can be found in the literature. The dependency of the clavicular abduction as function of the humeral elevation in the frontal plane was reported in [6]. The following simplified relationships were synthesized based on optical measurements of the human arm in the frontal (plane **x-z**), horizontal (plane **y-z**), and sagittal (plane **x-y**). They represent an idealistic status and serve as inputs for the mechanical design.

*The frontal plane*: We assumed that all rotations in the mechanism are zero except the abduction-adduction angles $s_A$ and $g_A$. We observed that the lower limit of angle $s_A$ depends on the angle of the humeral elevation $e_A$ as shown in Fig.2. Its minimum value is zero when the humeral elevation is zero.

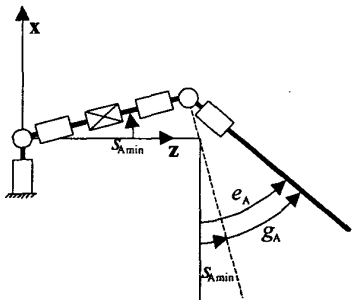


**Fig. 2**: *The shoulder motion in the frontal plane*

The lower limit of angle $g_A$ is dependent on the current value of angle $s_A$, while the shoulder expansion depends on the shoulder abduction angle as follows

$$s_T = (\tfrac{4}{5} + \tfrac{6}{5}\frac{s_A}{\pi}) s_{T0} \ . \qquad (1)$$

Note that all angles are measured in radians. Here, $s_{T0}$ is the length of the shoulder link when the shoulder abduction is zero. The shoulder link shortens by increasing $s_A$ and is about 80% of the initial value when $s_A$ reaches its upper limit. The lower and the upper limits of the moving coordinates are listed in Tb. 1.

| Coordinate | Lower limit | Upper limit |
|---|---|---|
| $e_A$ | $0$ | $\pi$ |
| $s_A$ | $\frac{1}{6}e_A$ | $\frac{1}{6}\pi$ |
| $g_A$ | $-s_A$ | $\frac{5}{6}\pi$ |
| $s_T = f(s_A)$ | $\frac{4}{5}s_{T0}$ | $s_{T0}$ |

**Tb. 1**: *The joint limits corresponding to the shoulder movements in the frontal plane*



Authorized licensed use limited to: Universita degli Studi di Genova. Downloaded on April 29,2023 at 14:43:20 UTC from IEEE Xplore. Restrictions apply.

*The horizontal plane*: We assumed that the changing rotations are the shoulder flexion-extension $s_F$ and the upper arm rotation $g_R$. The lower and the upper limit of both angles are independent, but the shoulder translation $s_T$ is a function of the rotation angle $s_F$

$$s_T = (\tfrac{4}{5} + \tfrac{6}{5}\tfrac{s_F}{\pi}) s_{T0} \ . \qquad (2)$$

The lower and the upper joint limits of the measured coordinates are listed in Tb. 2.

| Coordinate | Lower limit | Upper limit |
|---|---|---|
| $s_F$ | $-\frac{1}{6}\pi$ | $0$ |
| $g_R$ | $-\frac{1}{2}\pi$ | $\frac{1}{6}\pi$ |
| $s_T = f(s_F)$ | $\frac{4}{5}s_{T0}$ | $s_{T0}$ |

**Tb. 2**: *The joint limits corresponding to the shoulder movements in the horizontal plane*

*The sagittal plane*: The changing rotations were the shoulder rotation $s_R$ and the upper arm flexion-extension $g_F$. Their relationship appeared to be linear

$$s_R = \tfrac{1}{9} g_F \ . \qquad (3)$$

The joint limits are shown in Tb. 3.

| Coordinate | Lower limit | Upper limit |
|---|---|---|
| $s_R$ | $-\frac{1}{10}\pi$ | $\frac{1}{30}\pi$ |
| $g_F$ | $-\frac{9}{10}\pi$ | $\frac{9}{30}\pi$ |

**Tb. 3**: *The joint limits corresponding to the shoulder movements in the saggital plane*

The glenohumeral joint provides a great majority of the arm's motion ability. The range of motion in the sternoclavicular joint is only a few degrees. Nevertheless, the sternoclavicular joint plays an important role in the reachability of the arm. It serves for collision avoidance between the arm links and the body. If we fix the sternoclavicular joint, the motion of the arm will be troubled by collisions with the torso.

## 3 The humanoid shoulder designed by a fully parallel mechanism

The shoulder mechanism (the sternoclavicular joint and the shoulder link) has to support and orient the arm. Therefore, a serial mechanism in Fig. 1 may not be the best choice. Instead, we propose in this section a fully parallel mechanism, which can provide higher stiffness and more precise orientation [7]. It is understood that the base is fixed and corresponds to the body, while the movable platform supports the glenohumeral joint. The main kinematic parameters of this mechanism are illustrated in Fig. 3.

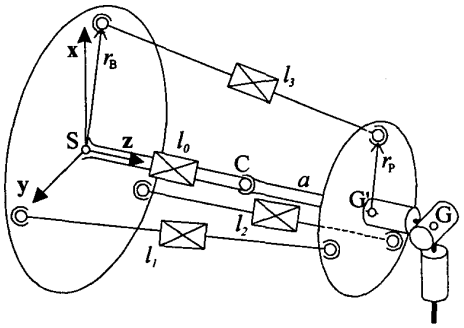


**Fig. 3**: *The shoulder modeled with a parallel mechanism*

The mechanism possesses four extendable legs. The translational joints are driven and the lengths $l_1, l_2, l_3, l_0$ are the joint coordinates. The three outer legs $l_1, l_2, l_3$ are attached to the base plane and to the platform plane via passive spherical joints. There is also a passive spherical joint C located in the central leg, which lies at a distance $a$ from the platform plane.

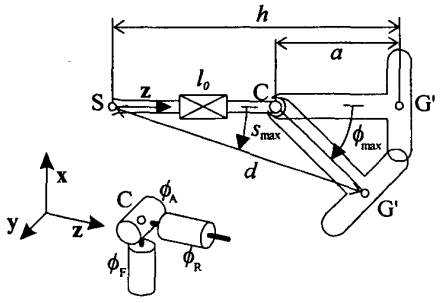


**Fig. 4**: *A side view of the platform's inclination*

The basic structure of the mechanism is symmetrical. The attachments of the outer legs are positioned on a circle of radius $r_B$ on the base side and on a circle of a radius $r_P$ on the platform side. The platform has four degrees of freedom. It can be placed in a desired orientation and expanded. The last, however, is intended to be dependent (via an imposed control law) in the sense



Authorized licensed use limited to: Universita degli Studi di Genova. Downloaded on April 29,2023 at 14:43:20 UTC from IEEE Xplore. Restrictions apply.

of coordinate $s_T$ in the serial mechanism (1). The spatial orientating of the platform is realized about the central spherical joint C.

Fig. 4 shows a longitudinal section of the mechanism in its maximum inclination. Here, $h$ is the size of the shoulder and will be used from now on as a unit to represent all distances. It is assumed that the maximum inclination angle $s_{max}$ is symmetric about axis **z**. Its value results from the ranges of angles $s_A$ and $s_F$. According to the range of translation $s_T$, we can also deduce length $d$. Ratio $\phi_{max}/s_{max}$ does not have a straightforward anatomical explanation. A higher $\phi_{max}$ introduces better orientation capabilities for the arm, a higher $s_{max}$ assures avoidance with the body. Tb. 4 lists the chosen values.

| $s_{max}$ | $\phi_{max}$ | $d$ | $r_B$ | $r_P$ |
|---|---|---|---|---|
| $\frac{1}{12}\pi$ | $\frac{21}{120}\pi$ | $\frac{4}{5}h$ | $\frac{8}{17}h$ | $\frac{4}{17}h$ |

**Tb. 4**: *Input parameters of the parallel mechanism*

When $\phi = 0 \Rightarrow l_0 = l_{0max}$ and $\phi = \phi_{max} \Rightarrow l_0 = l_{0min}$, the following is valid

$$a = \tfrac{4}{5}h\frac{\sin s_{max}}{\sin\phi_{max}}\ , \tag{4}$$

$$l_{0min} = \tfrac{4}{5}h\frac{\sin(\phi_{max} - s_{max})}{\sin\phi_{max}}\ , \tag{5}$$

$$l_{0max} = h - a\ . \tag{6}$$

From a mechanical viewpoint, it is desirable to implement a consistent overlapping in the actuator of the central leg (minimize $l_{0max} - l_{0min}$).

## 4 Kinematic analysis and sensitivity

Let vector $\mathbf{l}_0$ be associated with the central leg. We can compute the vectors of outer legs by

$$\mathbf{l}_i = \mathbf{l}_0 + \mathbf{T}_F\mathbf{T}_A\mathbf{T}_R\mathbf{p}_i - \mathbf{b}_i\ ,\ \text{where}\ \mathbf{l}_0 = (0,0,l_0)^T \tag{7}$$

and $i = 1,2,3$. Here, the following attachment points are introduced

$$\mathbf{b}_1 = (0, r_B, 0)^T,\ \mathbf{p}_1 = (0, r_P, a)^T\ , \tag{8}$$

$$\mathbf{b}_2 = (-\tfrac{\sqrt{3}}{2}r_B, -\tfrac{1}{2}r_B, 0)^T,\ \mathbf{p}_2 = (-\tfrac{\sqrt{3}}{2}r_P, -\tfrac{1}{2}r_P, a)^T, \tag{9}$$

$$\mathbf{b}_3 = (\tfrac{\sqrt{3}}{2}r_B, -\tfrac{1}{2}r_B, 0)^T,\ \mathbf{p}_3 = (\tfrac{\sqrt{3}}{2}r_P, -\tfrac{1}{2}r_P, a)^T\ . \tag{10}$$

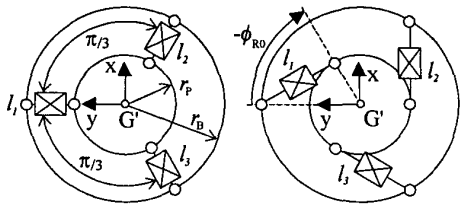


**Fig. 5**: *The upper view of the leg attachment points*

Transformation matrices $\mathbf{T}_F, \mathbf{T}_A, \mathbf{T}_R$ are associated with rotation angles $\phi_F$, $\phi_A$, $\phi_R$ about point C as shown in Fig. 4). These angles are the mechanism's external (Cartesian) coordinates

$$\mathbf{T}_F = \begin{bmatrix} 1 & 0 & 0 \\ 0 & c_F & -s_F \\ 0 & s_F & c_F \end{bmatrix},\ \mathbf{T}_A = \begin{bmatrix} c_A & 0 & s_A \\ 0 & 1 & 0 \\ -s_A & 0 & c_A \end{bmatrix},$$

$$\mathbf{T}_R = \begin{bmatrix} c_R & -s_R & 0 \\ s_R & c_R & 0 \\ 0 & 0 & 1 \end{bmatrix}, \tag{11}$$

where we mark $s_X = \sin\phi_X$ and $c_X = \cos\phi_X$. The lengths of legs $i = 1,2,3$ are the independent internal (joint) coordinates

$$l_i = \sqrt{\mathbf{l}_i^T\mathbf{l}_i}\ . \tag{12}$$

The length of the central leg depends on the inclination angle $\phi$. In order to achieve a smooth motion through the initial position we impose the following dependency

$$l_0 = l_{0min} + (l_{0max} - l_{0min})\cos(\tfrac{1}{2}\pi\frac{\phi}{\phi_{max}})\ , \tag{13}$$

$$\phi = \arccos(c_F c_A)\ . \tag{14}$$

The differential relationship of (7) can be expressed by

$$d\mathbf{l} = d\begin{bmatrix} l_1 \\ l_2 \\ l_3 \end{bmatrix} = \begin{bmatrix} \frac{\partial l_1}{\partial\phi_F} & \frac{\partial l_1}{\partial\phi_A} & \frac{\partial l_1}{\partial\phi_R} \\ \frac{\partial l_2}{\partial\phi_F} & \frac{\partial l_2}{\partial\phi_A} & \frac{\partial l_2}{\partial\phi_R} \\ \frac{\partial l_3}{\partial\phi_F} & \frac{\partial l_3}{\partial\phi_A} & \frac{\partial l_3}{\partial\phi_R} \end{bmatrix} d\begin{bmatrix} \phi_F \\ \phi_A \\ \phi_R \end{bmatrix} = \mathbf{J}d\begin{bmatrix} \phi_F \\ \phi_A \\ \phi_R \end{bmatrix}, \tag{15}$$

$$\frac{\partial l_i}{\partial\phi_F} = \frac{\mathbf{l}_i^T\frac{\partial\mathbf{l}_i}{\partial\phi_F}}{\sqrt{\mathbf{l}_i^T\mathbf{l}_i}}\ ,\ \frac{\partial\mathbf{l}_i}{\partial\phi_F} = \frac{\partial\mathbf{T}_F}{\partial\phi_F}\mathbf{T}_A\mathbf{T}_R\mathbf{p}_i\ , \tag{16}$$

$$\frac{\partial l_i}{\partial\phi_A} = \frac{\mathbf{l}_i^T\frac{\partial\mathbf{l}_i}{\partial\phi_A}}{\sqrt{\mathbf{l}_i^T\mathbf{l}_i}}\ ,\ \frac{\partial\mathbf{l}_i}{\partial\phi_A} = \mathbf{T}_F\frac{\partial\mathbf{T}_A}{\partial\phi_A}\mathbf{T}_R\mathbf{p}_i\ , \tag{17}$$



Authorized licensed use limited to: Universita degli Studi di Genova. Downloaded on April 29,2023 at 14:43:20 UTC from IEEE Xplore. Restrictions apply.

$$\frac{\partial l_i}{\partial \phi_R} = \frac{\mathbf{l}_i^T \frac{\partial \mathbf{l}_i}{\partial \phi_R}}{\sqrt{\mathbf{l}_i^T \mathbf{l}_i}}, \quad \frac{\partial \mathbf{l}_i}{\partial \phi_R} = \mathbf{T}_F \mathbf{T}_A \frac{\partial \mathbf{T}_R}{\partial \phi_R} \mathbf{p}_i, \qquad (18)$$

$i = 1,2,3$. The angular velocity of the platform and the linear velocities in the legs are related by

$$\omega = \begin{bmatrix} 1 & 0 & s_A \\ 0 & c_F & -s_F c_A \\ 0 & s_F & c_F c_A \end{bmatrix} \mathbf{J}^{-1} \frac{d\mathbf{l}}{dt}. \qquad (19)$$

Matrix **J** is singular when $\phi_F, \phi_A, \phi_R = 0$. In this singularity, the mechanism cannot produce any resistance to a moment about axis $\phi_R$. To avoid the singularity, we introduced a starting angle $\phi_{R0}$ and analyzed throughout the whole workspace the following norms

$$\delta_F = \sqrt{\frac{d\mathbf{l}^T}{d\phi_F} \frac{d\mathbf{l}}{d\phi_F}}, \; d\phi_A, d\phi_R = 0, \qquad (20)$$

$$\delta_A = \sqrt{\frac{d\mathbf{l}^T}{d\phi_A} \frac{d\mathbf{l}}{d\phi_A}}, \; d\phi_F, d\phi_R = 0, \qquad (21)$$

$$\delta_R = \sqrt{\frac{d\mathbf{l}^T}{d\phi_R} \frac{d\mathbf{l}}{d\phi_R}}, \; d\phi_F, d\phi_A = 0. \qquad (22)$$

The smallest values of these norms for all orientations $\phi_F, \phi_A, \phi_R$ in the workspace expressed in terms of $[h / \text{rad}]$, where $h$ is the size of the mechanism, obtained for different starting angles $\phi_{R0} = (-\frac{1}{2}\pi, 0)$ (given in [rad]) are plotted in Fig. 6. It is evident that norms $\delta_F$ and $\delta_A$ decrease by decreasing angle $\phi_{R0}$, while norm $\delta_R$ increases (the maximum is at about $\phi_{R0} = -\frac{3}{18}\pi$).

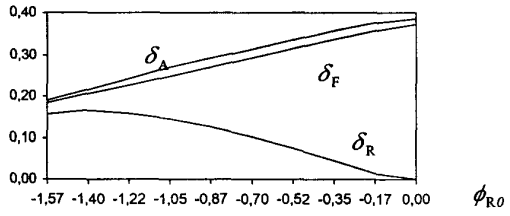


**Fig. 6**: *Norms (20-22) depending on the starting angle*

## 5 Leg lengths and interference

Leg lengths $l_i$, $i = 1,2,3$ were computed for all platform's orientations $\phi_F, \phi_A, \phi_R$ inside the workspace by the use of Eq. (7). Since the mechanism is symmetric, the minimum value $l_{imin}$ and the maximum value $l_{imax}$ are identical for all legs. They vary as functions of the starting angle $\phi_{R0}$. Lengths $l_{0min}$ and $l_{0max}$ are constant (see Eqs. 5-6). Once these values are known, we can estimate the overlapping of leg translations by

$$o_i = 2l_{imin} - l_{imax}, \; i = 0,\ldots,3. \qquad (23)$$

Fig. 7 shows the obtained $l_{imin}$, $l_{imax}$, and $o_i$, $i = 1,2,3$ in terms of the mechanism's size $h$.

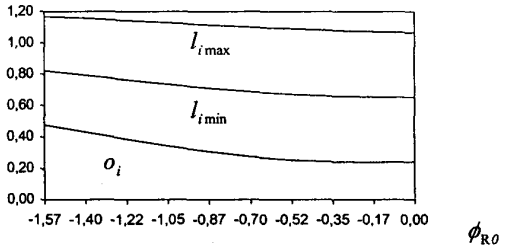


**Fig. 7**: *Minimum/maximum leg lengths and overlapping*

Possible interference (minimal distances) between legs were analyzed based on equations that formulate distance $L$ between two lines, first with end points $\mathbf{m}_1$, $\mathbf{m}_2$ and second with end points $\mathbf{n}_1$, $\mathbf{n}_2$

$$L = \sqrt{(\mathbf{m} - \mathbf{n})^T (\mathbf{m} - \mathbf{n})}, \qquad (25)$$

$$\mathbf{m} = \mathbf{m}_1 + k_m (\mathbf{m}_2 - \mathbf{m}_1), \qquad (26)$$

$$\mathbf{n} = \mathbf{n}_1 + k_n (\mathbf{n}_2 - \mathbf{n}_1), \qquad (27)$$

$$\begin{bmatrix} k_m \\ k_n \end{bmatrix} = \mathbf{Q}^{-1} \frac{(\mathbf{m}_1 - \mathbf{n}_1)^T (\mathbf{m}_2 - \mathbf{m}_1)}{(\mathbf{m}_1 - \mathbf{n}_1)^T (\mathbf{n}_2 - \mathbf{n}_1)}, \qquad (28,29)$$

$$\mathbf{Q} = \begin{bmatrix} -(\mathbf{m}_2 - \mathbf{m}_1)^T (\mathbf{m}_2 - \mathbf{m}_1) & (\mathbf{m}_2 - \mathbf{m}_1)^T (\mathbf{n}_2 - \mathbf{n}_1) \\ -(\mathbf{m}_2 - \mathbf{m}_1)^T (\mathbf{n}_2 - \mathbf{n}_1) & (\mathbf{n}_2 - \mathbf{n}_1)^T (\mathbf{n}_2 - \mathbf{n}_1) \end{bmatrix}.$$

To compute the distance between a point $\mathbf{n}$ and a line with end points $\mathbf{m}_1$, $\mathbf{m}_2$ Eqs. (25,26) were used, where

$$k_m = \frac{(\mathbf{m}_1 - \mathbf{n})^T (\mathbf{m}_2 - \mathbf{m}_1)}{(\mathbf{m}_2 - \mathbf{m}_1)^T (\mathbf{m}_2 - \mathbf{m}_1)}. \qquad (30)$$

Note that the end points of legs $i = 1,2,3$ are $\mathbf{b}_i$, $\mathbf{b}_i + \mathbf{l}_i$, of the lower part of leg *0* are $\mathbf{0}$, $\mathbf{l}_0$, while of the upper part of leg *0* are $\mathbf{l}_0$ and $\mathbf{l}_0 + \mathbf{T}_F \mathbf{T}_A \mathbf{T}_R (0,0,a)^T$. The minimum distances for all possible orientations inside the workspace between the outer legs $L_{ij}$, and between the outer legs and the central leg $L_{i0}$, in terms of mechanism's size $h$ are shown in Fig. 8.



Authorized licensed use limited to: Universita degli Studi di Genova. Downloaded on April 29,2023 at 14:43:20 UTC from IEEE Xplore. Restrictions apply.

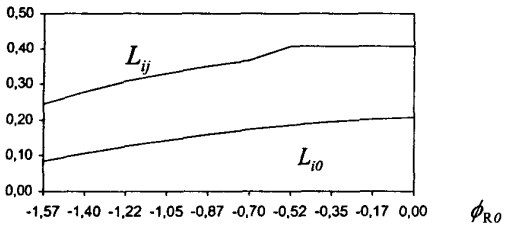


**Fig. 8**: *Minimum distances between mechanism's legs*

With respect to the dependencies in Figs. 6-8, one can select an ideal value $\phi_{R0}$ with the aim to avoid singularity and to simultaneously fulfill other mechanical restrictions in the shoulder's design. Our choice was $\phi_{R0} = -\frac{1}{3}\pi$. In the expected implementation of this parallel mechanism, the base will be attached to the body with an additional initial inclination (of axis **z**) upward and forward of about $\frac{1}{12}\pi$ radians.

Given the leg lengths $l_0$ and $l_i$, $i = 1,2,3$, we can compute for this mechanism the orientation angles $\phi_F$, $\phi_A$, $\phi_R$ in a closed-form [7,8]. Effective numerical solutions can also be found. Note that the direct kinematics problem is far more complex than the inverse kinematics. This mechanism possesses eight assemblies of legs of the same lengths. It means that for a given combination of the leg lengths the platform can accomplish eight different orientations $\phi_F$, $\phi_A$, $\phi_R$. Fortunately, within the imposed orientation limits and for the selected starting angle $\phi_{R0} = -\frac{1}{3}\pi$, we can find only one solution.

A physical model of the proposed parallel shoulder mechanism was built. The size corresponds to an average size of the human shoulder ($h = 17cm$). The picture with the indicated characteristic points is shown in Fig. 9.

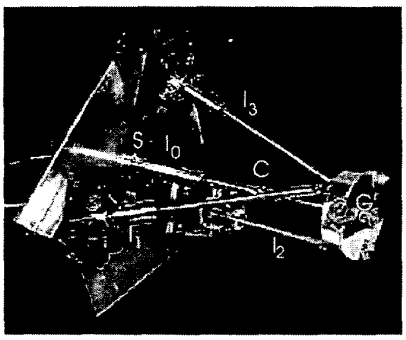


**Fig. 9**: *Physical model of the parallel shoulder mechanism*

## 6 Conclusions

Basic kinematic parameters of a fully parallel robotic mechanism that copies the human shoulder functions are reported. In the mechanism, four principal motions of the human shoulder were incorporated that provide the desired arm mobility and reachability. These are three rotations and one translation. The rotations represent the shoulder's flexion-extension, the shoulder's abduction-adduction, and the shoulder's rotation. The fourth degree of freedom is a translation associated with the shoulder enlargement-contraction along the medial-lateral axis. The mechanism is symmetric and doesn't suffer from singularities or leg collisions inside the imposed workspace.

## References

[1] V.M. Zatsiorsky, *Kinematics of Human Motion*, Human Kinetics Pub, 1997.

[2] Benati M.; Gaglio S.; Tagliasco V.; Zaccaria, R., "Anthropomorphic robotics," *Biological Cybern.*, vol 38, 1980, pp. 125-140.

[3] J. Lenarčič, A. Umek, "Simple model of human arm reachable workspace," *IEEE Trans on Syst. Man & Cybern.*, vol. 6, no. 4, 1994, pp. 1239-1246.

[4] J. Lenarčič, "Basic kinematic characteristics of humanoid manipulators," *Laboratory and Automat.*, vol. 11, 1999.

[5] A. Kacin, "Measurement of the human arm self-motion," *Diploma Thesis* (J. Lenarčič, adviser), Department of Physiotherapy, The University of Ljubljana, 1999, *in Slovenian.*

[6] A. Umek-Venturini, J. Lenarčič, "The kinematics of the human arm elevation in the frontal plane," *In Proc. 11th Int. Symp. on Biomedical Engineering*, Zagreb, Croatia, 1996, pp. 105-108.

[7] C. Innocenti, V. Parenti-Castelli, "Echelon form solution of direct kinematics for the general fully-parallel spherical wrist," *Mech Mach. Theory*, vol. 28, no. 4, 1993, 553-561.

[8] V. Parenti-Castelli, R. Di Gregorio, "Real-time actual pose determination of the general fully-parallel spherical wrist," *in Proc. of Mechanical Transmissions and Mechanisms '97*, China, 1997, pp. 895-899.



Authorized licensed use limited to: Universita degli Studi di Genova. Downloaded on April 29,2023 at 14:43:20 UTC from IEEE Xplore. Restrictions apply.